ACS Chemical Neuroscience

pubs.acs.org/chemneuro

Research Article

Putative Structures of Membrane-Embedded Amyloid β Oligomers

Aliasghar Sepehri and Themis Lazaridis*

Cite This: ACS Chem. Neurosci. 2023, 14, 99−110

Read Online

ACCESS | Metrics & More | Article Recommendations | Supporting Information

ABSTRACT: Perturbation of cell membranes by amyloid β (Ab) peptide oligomers is one possible mechanism of cytotoxicity in Alzheimer's disease, but the structure of such Ab−membrane complexes is unknown. Here we examine the stability of several putative structures by implicit membrane and all-atom molecular dynamics simulations. The structures include (a) a variety of models proposed by other researchers in the past, (b) a heptameric β barrel determined by grafting the Ab sequence onto α-hemolysin, (c) a similar structure with modified strand orientation and turn location based on an experimental β-hairpin structure, (d) oligomers inserting C-terminal β hairpins into one leaflet of the bilayer, (e) oligomers forming parallel C-terminal β barrels, and (f) a helical hexamer made of C-terminal fragments. The α-hemolysin-grafted structure and its alternately oriented variant are stable in the membrane and form an aqueous pore. In contrast, the C-terminal parallel barrels are not stable, presumably due to excessive hydrophobicity of their inner surface. The helical hexamer also failed to stabilize an aqueous pore for the same reason. The C-terminal hairpin-inserting structures remain stably inserted but, again, do not form an aqueous pore. Our results suggest that only β-barrels inserting a combination of C-terminal and other residues can form stable aqueous pores.

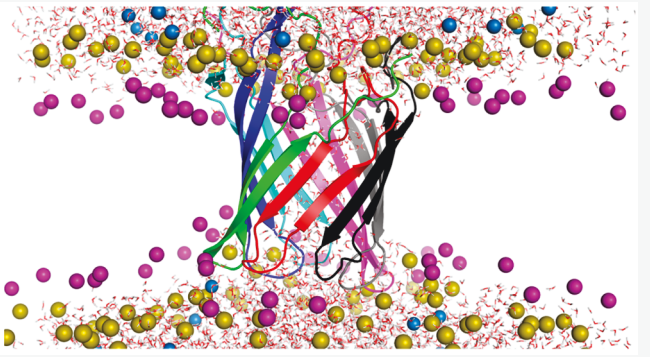

KEYWORDS: *Amyloid, Alzheimer's, molecular dynamics, ion channels, β-barrel, lipid bilayer*

INTRODUCTION

Amyloid β (Ab), a 39- to 43-residue peptide resulting from cleavage of a precursor protein, is the main constituent of the senile plaques that characterize Alzheimer's disease.[1] The 42-residue peptide tends to aggregate into fibrils faster and is more neurotoxic than the 1−40 variant.[2−4] While the peptide can take a partially helical conformation in some nonpolar environments,[5,6] it is primarily in β conformation in aqueous solution[7] and is more toxic in that conformation.[8] Several structures of fibrils have been determined, and all contain parallel β sheets.[9−17] Microcrystal structures of small fragments are also available, all in β conformation.[18,19] Ab is one of several peptides and proteins whose aggregation is linked to degenerative diseases.[20]

Soluble oligomers are reported to be more toxic than the monomer or the fibrils.[21−26] However, structural information on these toxic oligomers is scarce, low resolution, and sometimes in conflict.[27−33] Pyroglutamylated forms of Aβ, such as $A\beta pE_{3-42}$ and $A\beta pE_{3-40}$, are present in Alzheimer's disease brains in significant amounts (10−20% of total Aβ) and have emerged as the most cytotoxic Aβ species.[34−38] The second hallmark of Alzheimer's, tau aggregation, happens downstream of Aβ pathology and is likely caused by it.[39]

The link between Ab aggregation and disease has been heavily debated, and its interaction with cell membranes has received considerable attention. Many studies showed that amyloid β forms ion channels,[40−44] which are permeable to Ca^{2+} and lead to increase of its intracellular concentration. Alternatively, Ab oligomers could disrupt membranes via nonspecific defects.[45−47] Other work proposed that it is not the fibrils themselves but the *process* of fibril growth that damages membranes,[48−50] perhaps by lipid extraction.[51] Recent, low resolution cryo-ET showed oligomers attached and inserted into the outer leaflet of vesicles.[52] Much work has been done with fragments, especially 25−35, which is toxic in itself[53] and forms ion channels.[54,55] Some evidence of β-barrel structure in nonpolar environments exists,[56−58] although more recent work supported a flat tetramer in micelles.[59] Recently, the Ab sequence grafted onto α-hemolysin was shown by CryoEM to adopt a β-barrel structure.[60]

Several molecular models for Aβ ion channels have been proposed. Some are de novo constructions based on intuition and experimental constraints.[61,62] An elaborate and unusual 36-mer transmembrane structure with concentric barrels was found stable in short molecular dynamics (MD) simulations.[62]

Received: September 5, 2022
Accepted: December 2, 2022
Published: December 16, 2022

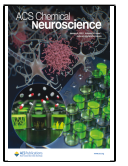

More recent work proposed concentric barrels for oligomers in solution.[63] Other models were based on the structure of the fibrils,[64−66] which, when subjected to MD simulations, broke up into distinct subunits. The insertion of such dimers and pentamers into the bilayer was also studied.[67] More recent models are β barrels inspired by recent results and using porins as templates.[68,69] Barrels also arose spontaneously in simulations of oligomers in solution.[70]

A recent publication from our lab examined structural pore models for IAPP.[71] Here we evaluate past models and generate new ones for full-length Ab using first implicit-membrane modeling to estimate thermodynamic stability and long all-atom simulations to estimate kinetic stability. We also evaluate the recent structure determined by cryoEM in a fusion construct with α-hemolysin[60] and a variant where the C-terminal (Ct) strand is flipped. We find that the Ct portion alone is able to anchor an oligomer onto the membrane but is too hydrophobic to sustain an aqueous pore. Only when more polar parts of the peptide are incorporated in the pore can an aqueous pore be stable.

RESULTS

Evaluation of Previous Models in Implicit Membrane. The oldest structural models for Ab ion channels were proposed by Guy and co-workers.[61] They were later revised based on newer experimental data.[62] No coordinates are available for these models, and they are difficult to reconstruct. Thus, we have not been able to evaluate them.

Models based on the original Ab fibril structures[11,79] were proposed by the Nussinov group. The most stable of these models are unsheared[64,65] or sheared[80] double layers with an inner layer composed of the 17−24 β strand and an outer layer composed of the 27−42 β strand. Because the barrel curvature creates a larger distance between the β strands in the outer layer, that layer is not H bonded. As a result, these barrels were observed to break into 4−6 subunits. We constructed a sheared 20-mer barrel according to the description of ref 80. The inner strands are at R = 15.5 Å and the outer strands at R ∼ 25 Å. A brief MD simulation of this model in a 15 Å implicit membrane cylindrical pore led to distortion in the shape of the inner barrel and disordering of the outer, Ct strands. Although it remains embedded, the transfer energy of this model from water to the pore is highly unfavorable (+141 kcal/mol) due to the outer strands, which, although hydrophobic, bury un-hydrogen-bonded backbone polar groups into a hydrophobic environment. Hence, we conclude that such models are not viable energetically.

Nguyen et al.[68] constructed a β barrel structure based on the data of Serra-Batiste et al.[57] and using PagP as a template. It consisted of a tetramer of hairpins (8 β strands in total) in NCCN antiparallel configuration (i.e., antiparallel hairpins interacting via their Ct strands). In this structure the peptides adopt two configurations: one is similar to PDB 7O1Q (see below) and the other is similar to the β hairpin structure of Hoyer et al.[81] We reconstructed the initial model based on the given information and the coordinates provided by the authors and subjected it to a 100 ps MD simulation in an R = 8 Å implicit toroidal pore. The model was reasonably stable, gave a favorable ΔW of −27 kcal/mol, but exhibited a break between segments A and D. The break is likely caused by the very tight side chain packing in the interior of this structure. A larger oligomer is likely to remain intact.

Ciudad et al.[59] determined the structure of Ab42 tetramers in DPC micelles (PDB 6RHY). Each tetramer contains a 6-stranded β sheet. The two edge molecules contribute two strands and the two central molecules contribute only one Ct strand and have the N-terminal strand disordered in solution. Two tetramers could form a β-sandwich octamer. It was proposed that these tetramers and octamers could make "edge pores", allowing ions to be conducted along their hydrated edges. MD simulations indeed showed water entering the membrane to hydrate the edges. However, the thermodynamic stability of these structures was not determined. The 6RHY structure in an IMM1 membrane gives a ΔW of +16 kcal/mol. In addition to the polar groups at the edges, it buries a His14, Gln15, and Lys16 into a nonpolar environment. An octamer made of two tetramers associating via the Gln15 face gives a ΔW of +27 kcal/mol. We suspect that this structure is stable in micelles, but in bilayers it rearranges, perhaps into a barrel. Preventing the desolvation of a few polar groups, such as the edge un-hydrogen-bonded backbone groups, might be enough to make the insertion free energy favorable.

The heptameric structure grafted onto α-hemolysin is a 14-stranded β barrel in which residues 7−42 form a β-hairpin.[60] This structure was extracted from the 7O1Q PDB file and subjected to a 100 ps MD simulation in an implicit toroidal pore (R_o = 11 Å, k = 10 Å). It was very stable with a ΔW of −11 kcal/mol. An alternative structure was constructed based on the Hoyer hairpin, PDB 2OTK,[81] which differs from the 7O1Q hairpin by flipping of the Ct strand and having the turn at residue 27 rather than at residue 24. The hairpin was first flattened (by restraining all Ca atoms to be near a plane) and then replicated and shifted to create a flat β sheet. That sheet naturally curved up upon MD simulation in implicit solvent. Finally, additional restraints between the edge strands were used to close the barrel. This heptamer was also very stable, giving an even more favorable ΔW of −31 kcal/mol.

Generation of Alternative Models and Evaluation in Implicit Membrane. The Ct third of Ab (residues 31−42) is very hydrophobic and thus most prone to interact with membranes (it is actually part of a transmembrane helix in the precursor protein). In solution a tendency has been reported for β hairpin formation at this part of the sequence.[82] Hence, we considered the possibility that several Ct hairpins come together to form a membrane-embedded β barrel. Residues 28−42 were aligned to our previous octameric protegrin barrel[83] in the following way (bold residues face outward):

RG**G**R**L**C**Y**CRRR**F**C**V**C**V**GR
KG**A**I**I**G**L**MV**G**G**V**V**I**A

The rest of the peptide was built in extended conformation in solution. This structure gave a favorable insertion energy into an implicit membrane pore. However, the length of the hairpins is not sufficient to cross the entire membrane.

We next considered the possibility that the Ct segments form a parallel β-barrel that crosses the entire membrane. Two oligomeric states were considered, 8mer and 16mer. First a β barrel from segments 31−42 was constructed by first making a flat β sheet with off-register H-bonds (shifted by one residue). The flat sheet developed a natural curvature during MD simulation in implicit water and was then forced to close by H bonding distance restraints. The rest of the peptide was added in an extended conformation. The initial structure was placed in an implicit membrane pore and relaxed for 200 ps with harmonic restraints on 30−42 backbone and 100 ps without. Both structures were stable in implicit membrane, with

https://doi.org/10.1021/acschemneuro.2c00535
ACS Chem. Neurosci. 2023, 14, 99−110

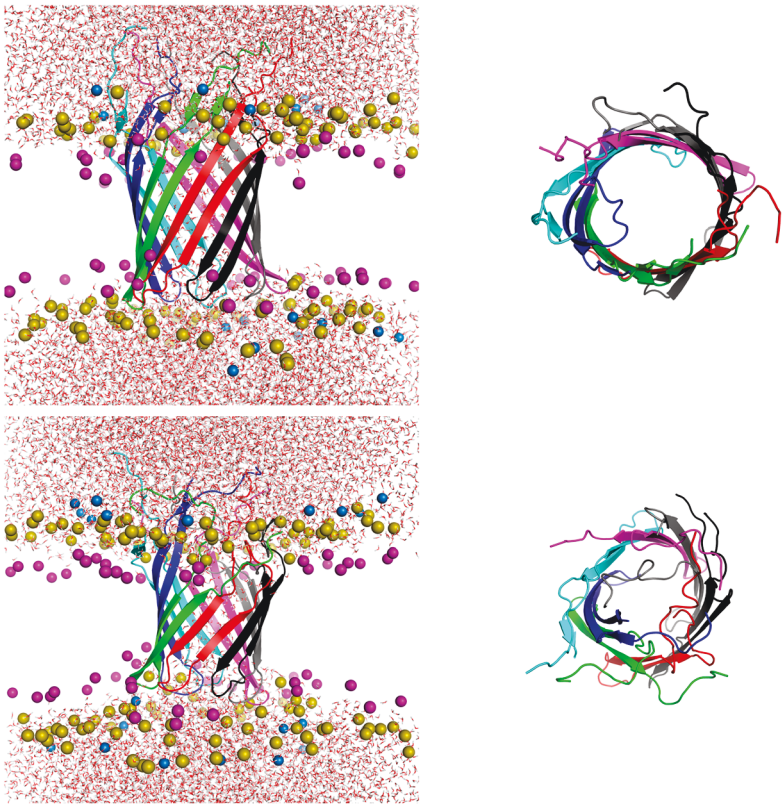

Figure 1. Structures of 7OQ1 at the beginning (top) and at the end (bottom) of the simulation. In the side views, there are peptides, water, and lipid headgroups which are phosphorus atoms of POPC (olive), O3 atoms in BGLC residue of GM1 (sky blue), and C1 atoms in cholesterol (purple). The top views only contain peptides.

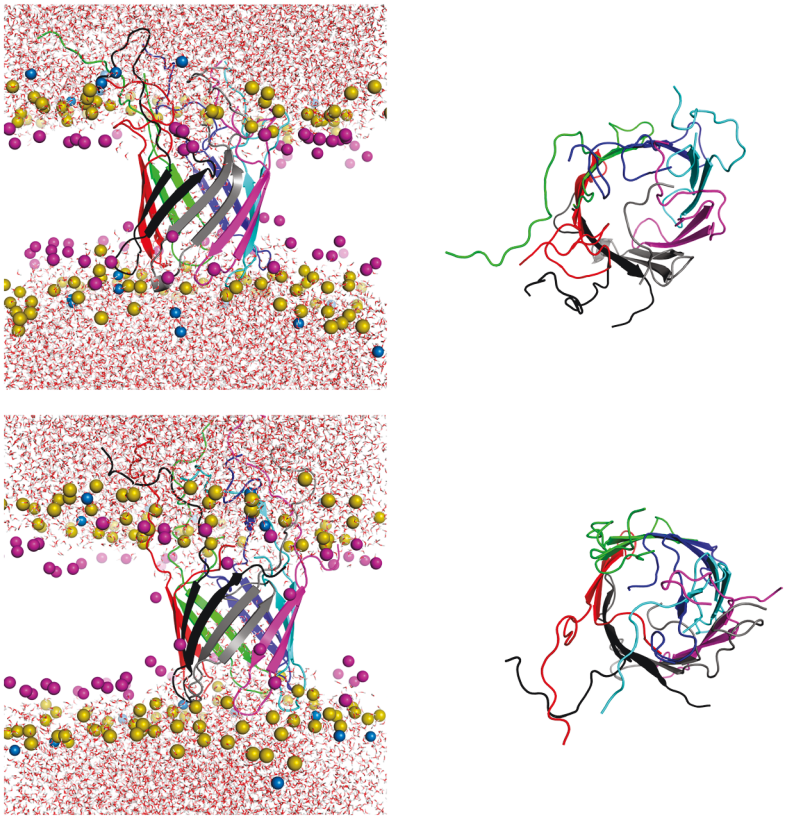

Figure 2. Structures of Hoyer 7mer at the beginning (top) and at the end (bottom) of the simulation. Colors are as in Figure 1.

https://doi.org/10.1021/acschemneuro.2c00535
ACS Chem. Neurosci. 2023, 14, 99−110

favorable ΔW (−96 kcal/mol for the 16mer and −45 kcal/mol for the 8mer). In the 8mer some helix content was added at residues 14−22 based on the structure of Ab40 in TFE/water (PDB 1AML[84]), to match recent FTIR results.[85]

It has been proposed that a fraction of Ab may remain in the membrane after cleavage of the precursor protein and interact with other membrane proteins.[86] Because the Ct part forms a TM helix in the precursor protein, it is conceivable that that portion might remain in the membrane as a helix despite the fact that it has been cleaved. We built residues 15−42 as an α helix and modeled it in implicit membrane. Its energy of insertion was slightly unfavorable (+4 kcal/mol) due to the burial of the C-terminus but remained in the membrane in 100 ps (there is a barrier to exit). Nevertheless, we considered the possibility that a number of these helices may come together to form a transient pore.

All-Atom Simulations. Based on the above results, we decided to subject the systems in Table 5 to all-atom simulations. The purpose of these simulations was to filter out structures that are clearly unstable. The target simulation time was 5 μs but the simulation was stopped if the peptides started to unfold and the pore to dissipate. Structures stable on this time scale, short by experimental standards, may or may not be stable on experimental time scales. But unstable structures can be clearly ruled out.

Figures 1 and 2 show initial (top) and final (bottom) structures of 7O1Q and Hoyer 7mer, respectively. Both pores, which on average contain ∼260 water molecules, are stable. However, many β strands of 7O1Q are shorter after the simulation; parts that are out of the membrane lose secondary structure and fold back from their initial extended conformation. This leads to backbone RMSD after 5 μs of 8.7 and 11.0 Å for 7O1Q and Hoyer 7mer, respectively. Plots of RMSD and secondary structure as a function of time can be found in Supporting Information.

In a stable pore the interactions between adjacent peptides are stronger than those between nonadjacent peptides.[71,87] We examined this on the two heptamers, where there are 21 interaction pairs, 7 adjacent and 14 nonadjacent. Table 1 shows the 10 strongest pair interactions that were calculated over the last 2 μs of each simulation. The average interaction energy over adjacent peptides is about −205 kcal/mol for 7O1Q and −136 kcal/mol for Hoyer. Thus, interpeptide interactions are clearly stronger in 7O1Q. To find the reason, we examined different residue−residue interactions between adjacent peptides, and the most important ones are presented in Table 2. In 7O1Q we observe very strong salt bridges, such as E22-K28 and D23-K28, and strong polar interactions, such as D23-S26 and D23-N27. In the Hoyer 7mer at least one residue in important pairs is nonpolar and that prevents strong interactions.

Table 1. Ten Strongest Protein−protein Interaction Energies (kcal/mol) Calculated over the Last 2 μs of Each Simulation[a]

	7O1Q		Hoyer 7mer	
1	F-G*	−264 ± 24	A-B*	−204 ± 20
2	A-B*	−234 ± 11	D-E*	−196 ± 12
3	G-A*	−216 ± 11	F-G*	−145 ± 9
4	C-D*	−212 ± 6	C-D*	−139 ± 12
5	B-C*	−173 ± 10	E-F*	−116 ± 8
6	D-E*	−172 ± 5	G-A*	−98 ± 5
7	E-F*	−163 ± 10	B-D	−84 ± 9
8	B-D	−63 ± 13	B-C*	−57 ± 5
9	E-G	−62 ± 13	A-E	−53 ± 22
10	C-E	−43 ± 4	B-G	−35 ± 6

[a]* denotes adjacent peptides (next to each other in the original barrel).

We have also calculated protein−lipid interaction energies for 7O1Q and Hoyer 7mer over the last 2 μs of each simulation (Table 3). For fair comparison, these energies were normalized by the number of each lipid type. In both cases, protein−POPC is the strongest interaction and protein−cholesterol the weakest. The interaction with POPC and GM1 is larger for the Hoyer 7mer than for 7O1Q, which is consistent with the larger implicit membrane transfer energy determined for the Hoyer structure.

Table 4 shows the residues that have the highest interaction energies with GM1. In the Hoyer 7mer, positively charged residues K28 and R5 interact strongly with GM1, which has a net charge of −1. K28 is in the β-sheet of 7O1Q and in the loop of Hoyer 7mer. So it can interact with GM1 only in the Hoyer structure. Another example is K16, whose side chain is directed toward the pore of 7O1Q and toward the membrane of Hoyer 7mer in a way that it interacts strongly with POPC. R5 is in the disordered aqueous region of both structures, but it can explore more space in the Hoyer structure, which has a longer N-terminal tail. N27 is in the loop in the Hoyer structure but deeper in the membrane in 7O1Q.

Figure 3 shows the octamer hairpin system in the beginning (top) and after 1.97 μs (bottom) of all-atom simulation, where the simulation was stopped. The eight hairpins, as well as the aqueous channel they surround, initially span only one leaflet of the membrane. At the end of equilibration the barrel is somewhat flattened. After 150 ns of production, peptide C almost leaves the pore and locates behind peptides B and D. Consequently, the number of water molecules in the pore decreases from ∼80 to ∼30. At 1.97 μs six hairpins form a flat β sandwich, with hairpin B capping one edge of the sandwich and hairpin C on top of the sandwich and almost parallel to the membrane. Very little water remains in the membrane at that point. The aqueous part moves further into solvent. It contains small parallel and antiparallel β sheets but remains disordered.

Figure 4 shows the initial (top) and final (bottom) structures of the octameric parallel barrel. After equilibration all water has left the pore. After 5 μs, the barrel flattens, four β-strands partially unfold, and two strands across the pore move closer to each other. In the aqueous region, some built-in helices remained small and one grew substantially to 5 turns. Some small intermolecular parallel and antiparallel β sheets were also formed. For the similar 16-mer, the initial pore contained more than 800 water molecules and remained hydrated during equilibration (Figure 5 top panels). However, some distortion in the barrel was already evident. After 4 μs, one side of the barrel essentially dissolved and three Ct entered the pore lumen (Figure 5 bottom panels). Although the pore remained hydrated, it is clear that the barrel is not stable.

Figure 6 shows two different initial structures of helical Ct after NAMD equilibration. In one of them, the helices spanned the membrane completely but buried some polar groups in the membrane (left) while in the other one the helices spanned two-thirds of the membrane and buried only the hydrophobic Ct portion (right). In both cases, the pore in the Ct portion dried up after equilibration. This is not surprising, since all of

https://doi.org/10.1021/acschemneuro.2c00535
ACS Chem. Neurosci. 2023, 14, 99−110

Table 2. Important Residue−Residue Interaction Energies (kcal/mol) in Adjacent Peptides for 7O1Q and Hoyer 7mer Calculated over the Last 2 μs of Each Simulation[a]

system	A-B	B-C	C-D	D-E
7O1Q	E22-K28, −54 ± 1	E22-K28, −55.7 ± 0.7	D23-K28, −44 ± 10	E22-K28, −36 ± 4
	K16-A42, −44 ± 6	F19-I31, −6.9 ± 0.1	E22-K28, −16 ± 8	D23-K28, −16 ± 7
	D23-S26, −23.6 ± 0.3	K16-G33, −6.1 ± 0.1	F19-I31, −7.1 ± 0.1	D23-S26, −10 ± 2
Hoyer	K16-A42, −33 ± 2	K16-G37, −8.1 ± 0.7	K16-A42, −19 ± 10	F19-V36, −7.1 ± 0.1
	K16-I41, −11 ± 1	F19-V36, −7.1 ± 0.1	F19-V36, −7.29 ± 0.04	D23-I31, −5.7 ± 0.1
	D23-K28, −5 ± 4	A21-L34, −5.5 ± 0.1	A21-L34, −5.43 ± 0.06	A21-L34, −5.6 ± 0.1

system	E-F	F-G	G-A
7O1Q	E22-K28, −51.9 ± 0.9	E22-K28, −36.5 ± 2.7	E22-K28, −46.2 ± 1.8
	D23-S26, −19.6 ± 1.9	F19-I31, −7.42 ± 0.06	D23-K28, −33.7 ± 7.5
	D23-N27, −9.6 ± 1.6	Q15-M35, −7.16 ± 0.13	D23-S26, −11.9 ± 2.3
Hoyer	F19-V36, −7.21 ± 0.02	A21-L34, −5.35 ± 0.05	K16-A42, −21 ± 7
	A21-L34, −5.47 ± 0.05	D23-I31, −4.9 ± 0.1	F19-V36, −7.2 ± 0.1
	D23-I31, −5.44 ± 0.15	F19-V36, −4.7 ± 0.3	L17-V39, −5.9 ± 0.7

[a]The first residue is from the first peptide and the second residue from the second peptide.

Table 3. Normalized Interaction Energies (kcal/mol) of Protein−Lipid in 7O1Q and Hoyer 7mer Calculated over the Last 2 μs of Each Simulation

protein−lipid	7O1Q	Hoyer 7mer
protein−POPC	−7.5 ± 0.2	−8.8 ± 0.2
protein−GM1	−3.4 ± 0.3	−6.5 ± 0.6
protein−cholesterol	−1.40 ± 0.04	−1.2 ± 0.1

Table 4. Important Residue-GM1 Interaction Energies (kcal/mol) in 7O1Q and Hoyer 7mer Calculated over the Last 2 μs of Each Simulation

7O1Q		Hoyer 7mer	
residue-GM1	energy	residue-GM1	energy
D1-GM1	−9.4 ± 2.8	K28-GM1	−32.2 ± 2.5
D23-GM1	−8.3 ± 1.5	R5-GM1	−23.3 ± 6.2
V24-GM1	−8.3 ± 1.5	N27-GM1	−13.0 ± 1.4

the last 14 residues in the Ct are nonpolar. Thus, longer all-atom simulations were not run on these systems.

DISCUSSION

This work examined a variety of structural models of Ab42 oligomers interacting with lipid bilayers, including some proposed previously and additional ones created here. Our main conclusion is that the hydrophobic Ct portion (residues 30−42) is able to anchor the oligomer to the membrane but cannot by itself sustain an aqueous pore. The only structures that form a stable water pore are those that bury a larger portion of the peptide, including polar residues from the middle part, residues 17−30. Among the two stable pore structures we simulated on a μs time scale, 7O1Q exhibits stronger interprotein interactions, but the barrel made of Hoyer hairpins[81] has stronger peptide−lipid interactions. It is not possible at this point to say which one is more stable. The NMR structure of a tetramer in micelles also contains two hairpins with the same strand orientation and turn location as Hoyer's but different sides of the strands H-bonded (36−15, 34−17, etc. for Hoyer and 37−16, 35−18, etc. for the tetramer).[59]

The only model that is experimentally supported so far is 7O1Q, the heptamer grafted onto α-hemolysin.[60] Indeed, we find this model to be stable and to support an aqueous pore. It is likely, however, that other structures also exist. The peptide may not adopt the same structure if its termini are not constrained by a larger protein. First, the oligomeric state in 7O1Q is fixed by the α-hemolysin scaffold, but it could be different, or heterogeneous, in the free peptides. Other biophysical results are not fully compatible with this structure. For example, the cryoET results show large portions out of the membrane.[52] These structures are similar to our 8mer that buries Ct hairpins. FTIR results found a significant portion of α-helix,[85] whereas this model is β and random coil. It is possible, however, that some helix could develop in the disordered N-terminal tails at longer time scales.

Many previous studies of Ab40 or Ab42 detected ion channel activity with cation selectivity[88−90] and the ability to conduct Ca^{2+}.[91] These channels were found to be blocked by Zn^{2+} [92,93] due to interaction with His13,14.[94] Among the two models that support an aqueous pore, 7O1Q has K16 and K28 in the pore lumen and E22, D23 near the loop. The Hoyer barrel has E22 in the lumen and K16, K28 in the loop or facing the exterior. Thus, the Hoyer barrel seems more compatible with cation selectivity. Both models have H13, 14 near the entrance of the pore where binding of Zn^{2+} could have an effect on conductance. Confirmation of this cation selectivity, and specifically the ability to conduct Ca^{2+}, could be done in future work by calculation of potentials of mean force for specific ions. There are, however, other experimental studies that found no selectivity.[45,95,96]

Certain sequence changes in Ab correlate with enhanced toxicity. For example, Ab42 is known to be more toxic than Ab40[2−4] and one study found ion channels formed by Ab42 but not Ab40,[96] contradicting earlier papers mentioned above. In the two stable barrel structures the last two residues are disordered and not part of the barrel. So they are unlikely to affect the stability of the final barrel structure. Similarly, the higher toxicity of the pyroglutamated variants,[34−38] which have a more hydrophobic N-terminus, cannot be accounted for by the barrel structures, where the N-terminus is disordered and far from the membrane. One possible explanation is that these changes do not affect the final state but lower the barrier for its formation by increasing the propensity for aggregation. Other mutation effects are also difficult to rationalize in the context of the barrel structures. For example, E22, which is in the pore lumen in the stable barrel structures, is often mutated to G, K, Q, or nothing in familial Alzheimer's cases.[97] The mechanisms

https://doi.org/10.1021/acschemneuro.2c00535
ACS Chem. Neurosci. 2023, 14, 99−110

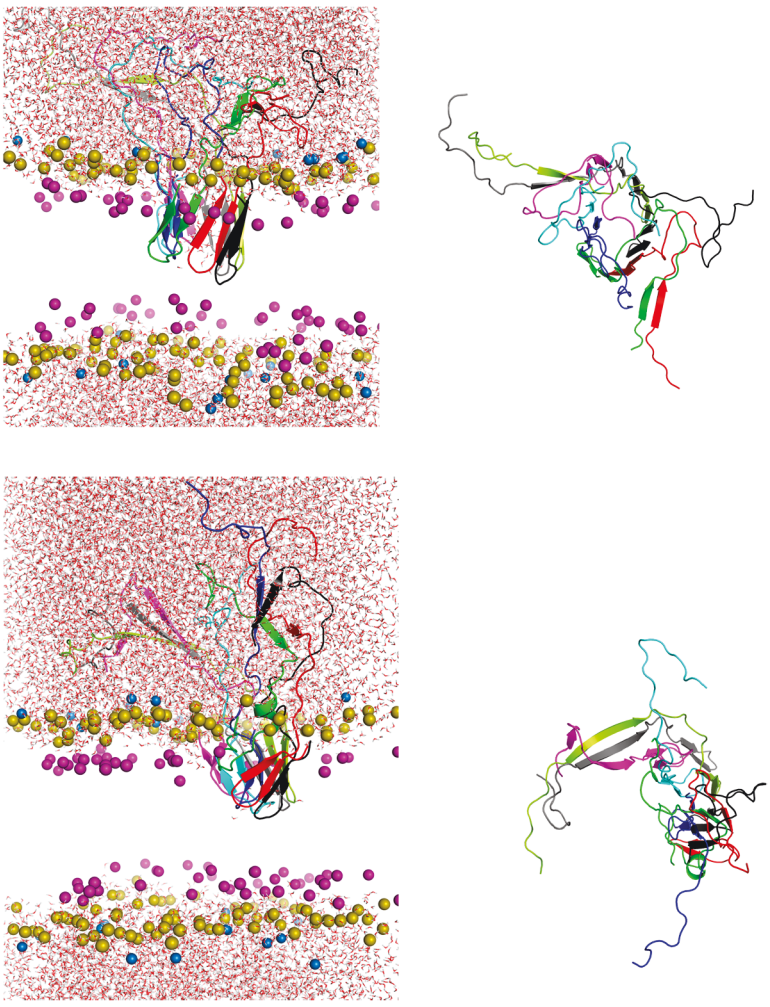

Figure 3. Structures of 8mer Ct hairpins at the beginning (top) and at the end (bottom) of the simulation. Peptide C is in red.

of this could be varied, such as loss of physiological function, effect on cleavage propensity, effect on aggregation propensity, etc.

We also considered the possibility that the Ct portion inserts into the membrane as an α-helix. However, this is thermodynamically unfavorable. In addition, because this portion is hydrophobic, there is no source of synergy when multiple helices come together. In preliminary simulations we saw the pore dry up. There are no polar residues that could support an aqueous pore. Nevertheless, a previous study found that a bundle of four helices could conduct Ca^{2+}, although no specific information on hydration was given.[98]

In the amyloid field it is well established that oligomers have varying toxicity.[99] What characteristics make some oligomers toxic and others nontoxic is not understood. Normally, oligomers formed in solution are expected to bury their hydrophobic residues, but kinetic trapping may prevent them from doing so completely. From the present results we could hypothesize that toxic are those oligomers that (a) expose enough hydrophobic surface area to interact with membranes and (b) contain β hairpins similar to those that form conducting barrels in the membrane. Alternatively, pores could be formed by monomers that encounter each other after binding to the membrane. A disulfide-stabilized version of the Hoyer hairpin was able to form toxic oligomers containing 40% β sheet but not fibrils.[100] Solid state NMR data in protofibrils formed by this molecule were consistent with hexameric barrels.[101] Our finding that this hairpin is able to form membrane-embedded barrels that can sustain an aqueous pore supports membrane permeabilization as a mechanism of toxicity.

Support for the β-barrel mechanism also comes from the existence of antibody A11, which recognizes not only toxic, prefibrillar oligomers of Ab and other amyloid-forming proteins such as α-synuclein and IAPP[102] but also β-barrel forming toxins, such as α-hemolysin and perforin.[103] Because the only solvent-exposed region of a β-barrel is the loops, it is possible that A11 recognizes the backbone conformation of the exposed loops in β-barrels. We can then infer that toxic oligomers contain β-hairpins in a conformation that exposes loops in similar ways as β-barrels.

METHODS

Implicit Membrane Model. For a rapid preliminary evaluation of putative structures we used the IMM1 implicit membrane model,[72] an extension of the EEF1 effective energy function for soluble proteins[73] to heterogeneous membrane−water systems. IMM1 uses a switching function that transitions smoothly from a nonpolar to an aqueous environment. Modeling of pores[74,75] is accomplished by making the switching function F dependent not only on the vertical (z)

https://doi.org/10.1021/acschemneuro.2c00535
ACS Chem. Neurosci. 2023, 14, 99−110

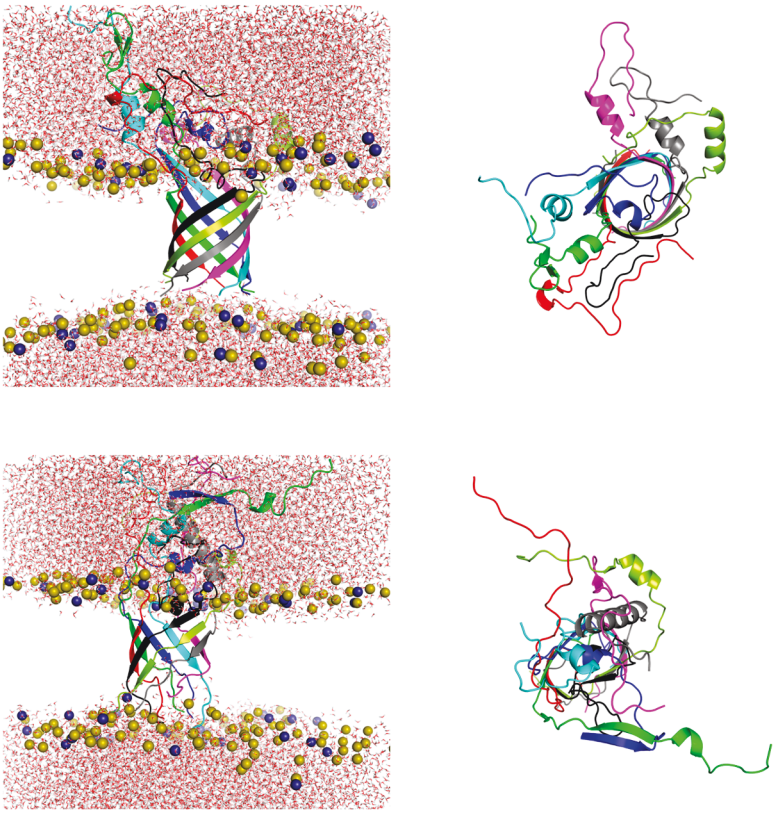

Figure 4. Structures of 8mer parallel Ct barrel at the beginning (top) and at the end (bottom) of the simulation.

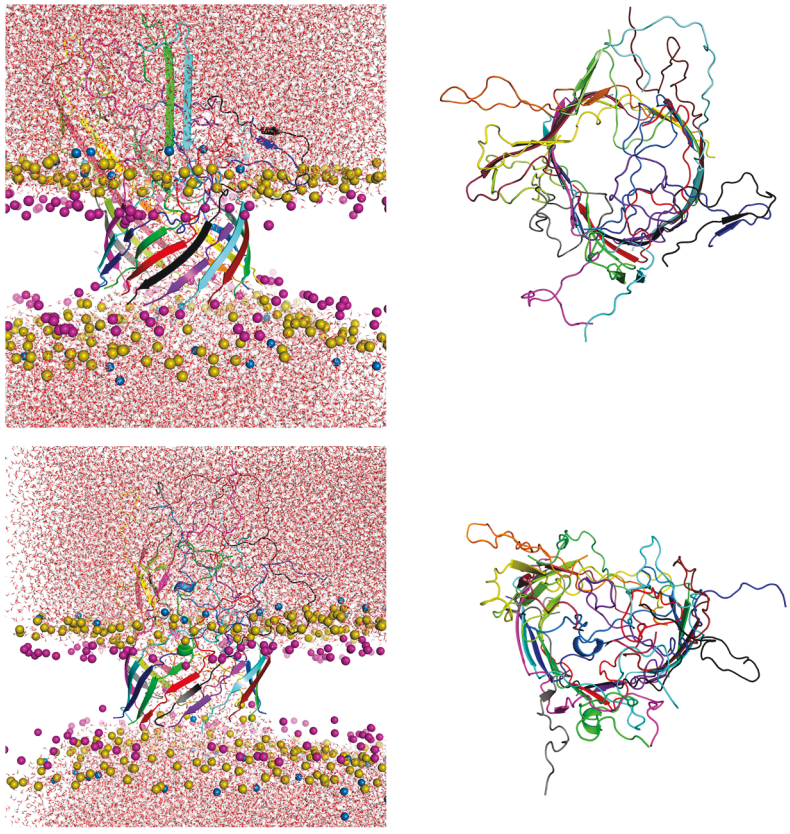

Figure 5. Structures of 16mer parallel Ct barrel at the beginning (top) and at the end (bottom) of the simulation.

https://doi.org/10.1021/acschemneuro.2c00535
ACS Chem. Neurosci. 2023, 14, 99−110

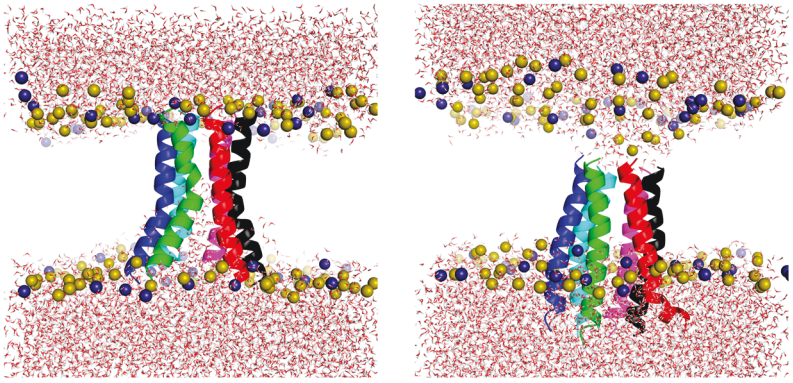

Figure 6. Structures of helical C-termini spanning the entire membrane (left) or two-thirds of the membrane (right) after NAMD equilibration.

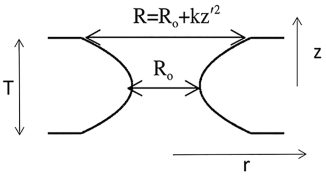

Figure 7. Shape of pores in an implicit membrane.

coordinate but also on the radial coordinate (the distance r from the z axis), as shown in Figure 7 and eq 1.

$$F(z', r') = f(z') + b(r') - f(z')b(r'), \quad f(z') = \frac{z'^n}{1 + z'^n},$$
$$b(r') = 1 - \frac{r'^n}{1 + r'^n}, \quad z' = |z|/(T/2), \quad r' = r/R \tag{1}$$

The shape of the pore can be specified by the dependence of R on z'. In cylindrical pores $R = R_o$, independent of z. Toroidal pores are approximated by the parabolic model $R = R_o + kz'^2$. An estimate of the stability of the pore is given by the transfer energy ΔW, which is the energy of transferring a given peptide structure from water to the implicit membrane pore. It should be noted, however, that this quantity does not include the free energy of membrane deformation and may thus overestimate pore stability. The implicit membrane model is highly approximate and cannot account for all the intricacies of complex peptide−water−lipid complexes. It only provides a rough, first estimate of the stability of a peptide on a membrane or a pore based on hydrophobic interactions and polar desolvation.

All-Atom Simulations. Table 5 lists properties of the systems subjected to all-atom simulations. In all of these, each peptide has 42 residues except the helical Ct that comprise residues 15−42. The initial configuration of peptides in each system was prepared with the implicit membrane model. Then, we used CHARMM-GUI to add lipids, with peptide/lipid ratio of 1:30, 22.5 Å thickness of water slabs, and 0.15 M KCl. The initial configuration was equilibrated with NAMD in several steps with restraints on the peptides' backbones, lipid headgroups, waters, and ions that were gradually relaxed leading to a 5 ns production run without restraints. The equilibrated system was run on the Anton supercomputer in the *NPT* ensemble at 1 bar and 310 K with the Nose−Hoover thermostat and the Martyna, Tobias, and Klein (MTK) barostat.[76] The last column in Table 5 shows the simulation time for different systems. The helical systems were not run on Anton because the pore dried up during equilibration. The time step was 2.5 fs except in the presence of GM1 lipid, where a smaller time step (1 fs) had to be used to prevent convergence errors. The membranes were either 20% or 30% POPG in POPC or more biologically relevant mixtures of POPC, cholesterol, and the ganglioside GM1, which has been reported to interact with Ab and favor its insertion into the membrane.[77,78] The composition 60:30:10 was chosen to be similar to recent work,[52] with the GM1 slightly enhanced to improve the statistics of interaction with the peptides. The number of lipids was chosen to provide at least two

Table 5. Systems Simulated

system	number of peptides	atoms	waters	ions	lower leaflet $Z < 0$	upper leaflet $Z > 0$	time (μs)
7O1Q	7	88077	19007	93 K^+	64 POPC	62 POPC	5
				51 Cl^-	31 Chol	32 Chol	
					10 GM1	11 GM1	
Hoyer	7	85005	17985	90 K^+	66 POPC	60 POPC	5
				48 Cl^-	33 Chol	30 Chol	
					11 GM1	10 GM1	
8mer Ct hairpins	8	103773	22759	108 K^+	75 POPC	69 POPC	1.97
				60 Cl^-	41 Chol	31 Chol	
					14 GM1	10 GM1	
8mer parallel Ct barrel	8	96113	19699	124 K^+	94 POPC	98 POPC	5
				52 Cl^-	23 POPG	25 POPG	
16mer parallel Ct barrel	16	226179	51715	237 K^+	141 POPC	147 POPC	4
				141 Cl^-	71 Chol	73 Chol	
					23 GM1	25 GM1	
helical C-termini (residues 15−42)	6	55388	9688	79 K^+	61 POPC	65 POPC	
				25 Cl^-	25 POPG	29 POPG	
helical C-termini, half pore (residues 15−42)	6	60838	11502	83 K^+	60 POPC	66 POPC	
				29 Cl^-	24 POPG	30 POPG	

https://doi.org/10.1021/acschemneuro.2c00535
ACS Chem. Neurosci. 2023, 14, 99−110

layers of coverage around the peptides. All barrels were initially placed with their axis parallel to the membrane normal.

■ ASSOCIATED CONTENT

Supporting Information

The Supporting Information is available free of charge at https://pubs.acs.org/doi/10.1021/acschemneuro.2c00535.

Plots of root mean square deviation and secondary structure as a function of time (PDF)

Zip file with PDB files displayed in Figures 1−6 (ZIP)

■ AUTHOR INFORMATION

Corresponding Author

Themis Lazaridis − *Department of Chemistry, City College of New York, CUNY, New York, New York 10031, United States; Graduate Programs in Chemistry, Biochemistry, and Physics, The Graduate Center, City University of New York, New York, New York 10016, United States;* orcid.org/0000-0003-4218-7590; Phone: (212) 650-8364; Email: tlazaridis@ccny.cuny.edu

Author

Aliasghar Sepehri − *Department of Chemistry, City College of New York, CUNY, New York, New York 10031, United States*

Complete contact information is available at: https://pubs.acs.org/10.1021/acschemneuro.2c00535

Author Contributions

T.L. conceived the project. A.S. performed the simulations and the analysis of the results. T.L. wrote the manuscript with input from A.S.

Notes

The authors declare no competing financial interest.

■ ACKNOWLEDGMENTS

This work was supported by the National Science Foundation (Grant MCB-1855942). We thank Dr. Derreumaux for providing coordinates of their tetrameric models and Drs. J. Luo and S. Tatulian for comments on the manuscript. Anton computer time was provided by the Pittsburgh Supercomputing Center through Grant R01GM116961 from the NIH. The Anton machine at PSC was generously made available by D. E. Shaw Research, and computer time was provided by the National Center for Multiscale Modeling of Biological Systems through Grant P41GM103712-S1 from the NIH and Pittsburgh Supercomputing Center.

■ REFERENCES

(1) Hardy, J.; Allsop, D. Amyloid Deposition as the Central Event in the Aetiology of Alzheimer's Disease. *Trends Pharmacol. Sci.* **1991**, *12*, 383−388.

(2) Jarrett, J. T.; Berger, E. P.; Lansbury, P. T. The Carboxy Terminus of the β Amyloid Protein Is Critical for the Seeding of Amyloid Formation: Implications for the Pathogenesis of Alzheimer's Disease. *Biochemistry* **1993**, *32* (18), 4693−4697.

(3) Selkoe, D. J. Translating Cell Biology into Therapeutic Advances in Alzheimer's Disease. *Nature* **1999**, *399* (Suppl.), A23−A31.

(4) Kim, W.; Hecht, M. H. Sequence Determinants of Enhanced Amyloidogenicity of Alzheimer Aβ42 Peptide Relative to Aβ40. *J. Biol. Chem.* **2005**, *280* (41), 35069−35076.

(5) Barrow, C. J.; Zagorski, M. G. Solution Structures of β Peptide and Its Constituent Fragments: Relation to Amyloid Deposition. *Science* **1991**, *253* (5016), 179−182.

(6) Talafous, J.; Marcinowski, K. J.; Klopman, G.; Zagorski, M. G. Solution Structure of Residues 1−28 of the Amyloid β-Peptide. *Biochemistry* **1994**, *33* (25), 7788−7796.

(7) Barrow, C. J.; Yasuda, A.; Kenny, P. T. M.; Zagorski, M. G. Solution Conformations and Aggregational Properties of Synthetic Amyloid β-Peptides of Alzheimer's Disease. Analysis of Circular Dichroism Spectra. *J. Mol. Biol.* **1992**, *225* (4), 1075−1093.

(8) Simmons, L. K.; May, P. C.; Tomaselli, K. J.; Rydel, R. E.; Fuson, K. S.; Brigham, E. F.; Wright, S.; Lieberburg, I.; Becker, G. W.; Brems, D. N.; et al. Secondary Structure of Amyloid β Peptide Correlates with Neurotoxic Activity in Vitro. *Mol. Pharmacol.* **1994**, *45* (3), 373−379.

(9) Tycko, R. Solid-State NMR Studies of Amyloid Fibril Structure. *Annu. Rev. Phys. Chem.* **2011**, *62*, 279−299.

(10) Qiang, W.; Yau, W. M.; Luo, Y.; Mattson, M. P.; Tycko, R. Antiparallel β-Sheet Architecture in Iowa-Mutant β-Amyloid Fibrils. *Proc. Natl. Acad. Sci. U. S. A.* **2012**, *109* (12), 4443−4448.

(11) Luhrs, T.; Ritter, C.; Adrian, M.; Riek-loher, D.; Bohrmann, B.; Dobeli, H.; Schubert, D.; Riek, R. 3D Structure of Alzheimer's Amyloid-β(1−42) Fibrils. *Proc. Natl. Acad. Sci. U. S. A.* **2005**, *102* (48), 17342−17347.

(12) Schmidt, M.; Rohou, A.; Lasker, K.; Yadav, J. K.; Schiene-Fischer, C.; Fändrich, M.; Grigorieff, N. Peptide Dimer Structure in an Aβ(1-42) Fibril Visualized with Cryo-EM. *Proc. Natl. Acad. Sci. U. S. A.* **2015**, *112* (38), 11858−11863.

(13) Xiao, Y.; Ma, B.; McElheny, D.; Parthasarathy, S.; Long, F.; Hoshi, M.; Nussinov, R.; Ishii, Y. Aβ(1-42) Fibril Structure Illuminates Self-Recognition and Replication of Amyloid in Alzheimer's Disease. *Nat. Struct. Mol. Biol.* **2015**, *22* (6), 499−505.

(14) Wälti, M. A.; Ravotti, F.; Arai, H.; Glabe, C. G.; Wall, J. S.; Böckmann, A.; Güntert, P.; Meier, B. H.; Riek, R. Atomic-Resolution Structure of a Disease-Relevant Aβ(1-42) Amyloid Fibril. *Proc. Natl. Acad. Sci. U. S. A.* **2016**, *113* (34), E4976−E4984.

(15) Colvin, M. T.; Silvers, R.; Frohm, B.; Su, Y.; Linse, S.; Griffin, R. G. High Resolution Structural Characterization of Aβ42 Amyloid Fibrils by Magic Angle Spinning NMR. *J. Am. Chem. Soc.* **2015**, *137* (23), 7509−7518.

(16) Colvin, M. T.; Silvers, R.; Ni, Q. Z.; Can, T. V.; Sergeyev, I.; Rosay, M.; Donovan, K. J.; Michael, B.; Wall, J.; Linse, S.; et al. Atomic Resolution Structure of Monomorphic Aβ42 Amyloid Fibrils. *J. Am. Chem. Soc.* **2016**, *138* (30), 9663−9674.

(17) Gremer, L.; Schölzel, D.; Schenk, C.; Reinartz, E.; Labahn, J.; Ravelli, R. B. G.; Tusche, M.; Lopez-iglesias, C.; Hoyer, W.; Heise, H.; et al. Fibril Structure of Amyloid-Beta(1-42) by Cryo − Electron Microscopy. *Science* **2017**, *358* (6359), 116−119.

(18) Sawaya, M. R.; Sambashivan, S.; Nelson, R.; Ivanova, M. I.; Sievers, S. A.; Apostol, M. I.; Thompson, M. J.; Balbirnie, M.; Wiltzius, J. J. W.; McFarlane, H. T.; et al. Atomic Structures of Amyloid Cross-β Spines Reveal Varied Steric Zippers. *Nature* **2007**, *447* (7143), 453−457.

(19) Colletier, J. P.; Laganowsky, A.; Landau, M.; Zhao, M.; Soriaga, A. B.; Goldschmidt, L.; Flot, D.; Cascio, D.; Sawaya, M. R.; Eisenberg, D. Molecular Basis for Amyloid-β Polymorphism. *Proc. Natl. Acad. Sci. U. S. A.* **2011**, *108* (41), 16938−16943.

(20) Nguyen, P. H.; Ramamoorthy, A.; Sahoo, B. R.; Zheng, J.; Faller, P.; Straub, J. E.; Dominguez, L.; Shea, J. E.; Dokholyan, N. V.; de Simone, A.; et al. Amyloid Oligomers: A Joint Experimental/Computational Perspective on Alzheimer's Disease, Parkinson's Disease, Type II Diabetes, and Amyotrophic Lateral Sclerosis. *Chem. Rev.* **2021**, *121* (4), 2545−2647.

(21) Lambert, M. P.; Barlow, A. K.; Chromy, B. A.; Edwards, C.; Freed, R.; Liosatos, M.; Morgan, T. E.; Rozovsky, I.; Trommer, B.; Viola, K. L.; et al. Diffusible, Nonfibrillar Ligands Derived from Aβ1-42 Are Potent Central Nervous System Neurotoxins. *Proc. Natl. Acad. Sci. U. S. A.* **1998**, *95* (11), 6448−6453.

(22) Walsh, D. M.; Klyubin, I.; Fadeeva, J. V.; Cullen, W. K.; Anwyl, R.; Wolfe, M. S.; Rowan, M. J.; Selkoe, D. J. Naturally Secreted Oligomers of Amyloid β Protein Potently Inhibit Hippocampal Long-Term Potentiation in Vivo. *Nature* **2002**, *416* (6880), 535−539.
(23) Haass, C.; Selkoe, D. J. Soluble Protein Oligomers in Neurodegeneration: Lessons from the Alzheimer's Amyloid β-Peptide. *Nat. Rev. Mol. Cell Biol.* **2007**, *8* (2), 101−112.
(24) Bernstein, S. L.; Dupuis, N. F.; Lazo, N. D.; Wyttenbach, T.; Condron, M. M.; Bitan, G.; Teplow, D. B.; Shea, J. E.; Ruotolo, B. T.; Robinson, C. V.; et al. Amyloid-β 2 Protein Oligomerization and the Importance of Tetramers and Dodecamers in the Aetiology of Alzheimer's Disease. *Nat. Chem.* **2009**, *1* (4), 326−331.
(25) Bieschke, J.; Herbst, M.; Wiglenda, T.; Friedrich, R. P.; Boeddrich, A.; Schiele, F.; Kleckers, D.; Lopez Del Amo, J. M.; Grüning, B. A.; Wang, Q.; et al. Small-Molecule Conversion of Toxic Oligomers to Nontoxic β-Sheet-Rich Amyloid Fibrils. *Nat. Chem. Biol.* **2012**, *8* (1), 93−101.
(26) Haupt, C.; Leppert, J.; Rönicke, R.; Meinhardt, J.; Yadav, J. K.; Ramachandran, R.; Ohlenschläger, O.; Reymann, K. G.; Görlach, M.; Fändrich, M. Structural Basis of β-Amyloid-Dependent Synaptic Dysfunctions. *Angew. Chem., Int. Ed.* **2012**, *51* (7), 1576−1579.
(27) Cerf, E.; Sarroukh, R.; Tamamizu-Kato, S.; Breydo, L.; Derclaye, S.; Dufrêne, Y. F.; Narayanaswami, V.; Goormaghtigh, E.; Ruysschaert, J. M.; Raussens, V. Antiparallel β-Sheet: A Signature Structure of the Oligomeric Amyloid β-Peptide. *Biochem. J.* **2009**, *421* (3), 415−423.
(28) Parthasarathy, S.; Inoue, M.; Xiao, Y.; Matsumura, Y.; Nabeshima, Y. I.; Hoshi, M.; Ishii, Y. Structural Insight into an Alzheimer's Brain-Derived Spherical Assembly of Amyloid β by Solid-State NMR. *J. Am. Chem. Soc.* **2015**, *137* (20), 6480−6483.
(29) Ahmed, M.; Davis, J.; Aucoin, D.; Sato, T.; Ahuja, S.; Aimoto, S.; Elliott, J. I.; Van Nostrand, W. E.; Smith, S. O. Structural Conversion of Neurotoxic Amyloid-B 1−42 Oligomers to Fibrils. *Nat. Struct. Mol. Biol.* **2010**, *17* (5), 561−567.
(30) Gao, Y.; Guo, C.; Watzlawik, J. O.; Randolph, P. S.; Lee, E. J.; Huang, D.; Stagg, S. M.; Zhou, H. X.; Rosenberry, T. L.; Paravastu, A. K. Out-of-Register Parallel β-Sheets and Antiparallel β-Sheets Coexist in 150-KDa Oligomers Formed by Amyloid-β(1−42). *J. Mol. Biol.* **2020**, *432* (16), 4388−4407.
(31) Yu, L.; Edalji, R.; Harlan, J. E.; Holzman, T. F.; Lopez, A. P.; Labkovsky, B.; Hillen, H.; Barghorn, S.; Ebert, U.; Richardson, P. L.; et al. Structural Characterization of a Soluble Amyloid β-Peptide Oligomer. *Biochemistry* **2009**, *48* (9), 1870−1877.
(32) Stroud, J. C.; Liu, C.; Teng, P. K.; Eisenberg, D. Toxic Fibrillar Oligomers of Amyloid-β Have Cross-β Structure. *Proc. Natl. Acad. Sci. U. S. A.* **2012**, *109* (20), 7717−7722.
(33) Sarkar, B.; Mithu, V. S.; Chandra, B.; Mandal, A.; Chandrakesan, M.; Bhowmik, D.; Madhu, P. K.; Maiti, S. Significant Structural Differences between Transient Amyloid-β Oligomers and Less-Toxic Fibrils in Regions Known to Harbor Familial Alzheimer's Mutations. *Angew. Chem., Int. Ed.* **2014**, *53* (27), 6888−6892.
(34) Jawhar, S.; Wirths, O.; Bayer, T. A. Pyroglutamate Amyloid-β (Aβ): A Hatchet Man in Alzheimer Disease. *J. Biol. Chem.* **2011**, *286* (45), 38825−38832.
(35) Nussbaum, J. M.; Schilling, S.; Cynis, H.; Silva, A.; Swanson, E.; Wangsanut, T.; Tayler, K.; Wiltgen, B.; Hatami, A.; Rönicke, R.; et al. Prion-like Behaviour and Tau-Dependent Cytotoxicity of Pyroglutamylated Amyloid-β. *Nature* **2012**, *485* (7400), 651−655.
(36) Sofola-Adesakin, O.; Khericha, M.; Snoeren, I.; Tsuda, L.; Partridge, L. PGluAβ Increases Accumulation of Aβ in Vivo and Exacerbates Its Toxicity. *Acta Neuropathol. Commun.* **2016**, *4* (1), 109.
(37) Scheidt, H. A.; Adler, J.; Zeitschel, U.; Höfling, C.; Korn, A.; Krueger, M.; Roßner, S.; Huster, D. Pyroglutamate-Modified Amyloid β (11- 40) Fibrils Are More Toxic than Wildtype Fibrils but Structurally Very Similar. *Chem.—Eur. J.* **2017**, *23* (62), 15834−15838.
(38) Goldblatt, G.; Cilenti, L.; Matos, J. O.; Lee, B.; Ciaffone, N.; Wang, Q. X.; Tetard, L.; Teter, K.; Tatulian, S. A. Unmodified and Pyroglutamylated Amyloid β Peptides Form Hypertoxic Hetero-Oligomers of Unique Secondary Structure. *FEBS J.* **2017**, *284* (9), 1355−1369.
(39) Selkoe, D. J. Treatments for Alzheimer's Disease Emerge. *Science* **2021**, *373* (6555), 624−626.
(40) Arispe, N.; Rojas, E.; Pollard, H. B. Alzheimer Disease Amyloid β Protein Forms Calcium Channels in Bilayer Membranes: Blockade by Tromethamine and Aluminum. *Proc. Natl. Acad. Sci. U. S. A.* **1993**, *90* (2), 567−571.
(41) Demuro, A.; Smith, M.; Parker, I. Single-Channel Ca2+ Imaging Implicates Aβ 1−42 Amyloid Pores in Alzheimer's Disease Pathology. *J. Cell Biol.* **2011**, *195* (3), 515−524.
(42) Lal, R.; Lin, H.; Quist, A. P. Amyloid Beta Ion Channel: 3D Structure and Relevance to Amyloid Channel Paradigm. *Biochim. Biophys. Acta, Biomembr.* **2007**, *1768* (8), 1966−1975.
(43) Kagan, B. L.; Azimov, R.; Azimova, R. Amyloid Peptide Channels. *J. Membr. Biol.* **2004**, *202* (1), 1−10.
(44) Prangkio, P.; Yusko, E. C.; Sept, D.; Yang, J.; Mayer, M. Multivariate Analyses of Amyloid-Beta Oligomer Populations Indicate a Connection between Pore Formation and Cytotoxicity. *PLoS One* **2012**, *7* (10), e47261.
(45) Kayed, R.; Sokolov, Y.; Edmonds, B.; McIntire, T. M.; Milton, S. C.; Hall, J. E.; Glabe, C. G. Permeabilization of Lipid Bilayers Is a Common Conformation-Dependent Activity of Soluble Amyloid Oligomers in Protein Misfolding Diseases. *J. Biol. Chem.* **2004**, *279* (45), 46363−46366.
(46) de Planque, M. R. R.; Raussens, V.; Contera, S. A.; Rijkers, D. T. S.; Liskamp, R. M. J.; Ruysschaert, J. M.; Ryan, J. F.; Separovic, F.; Watts, A. β-Sheet Structured β-Amyloid(1-40) Perturbs Phosphatidylcholine Model Membranes. *J. Mol. Biol.* **2007**, *368* (4), 982−997.
(47) Valincius, G.; Heinrich, F.; Budvytyte, R.; Vanderah, D. J.; McGillivray, D. J.; Sokolov, Y.; Hall, J. E.; Lösche, M. Soluble Amyloid β-Oligomers Affect Dielectric Membrane Properties by Bilayer Insertion and Domain Formation: Implications for Cell Toxicity. *Biophys. J.* **2008**, *95* (10), 4845−4861.
(48) Yip, C. M.; McLaurin, J. Amyloid-β Peptide Assembly: A Critical Step in Fibrillogenesis and Membrane Disruption. *Biophys. J.* **2001**, *80* (3), 1359−1371.
(49) Wogulis, M.; Wright, S.; Cunningham, D.; Chilcote, T.; Powell, K.; Rydel, R. E. Nucleation-Dependent Polymerization Is an Essential Component of Amyloid-Mediated Neuronal Cell Death. *J. Neurosci.* **2005**, *25* (5), 1071−1080.
(50) Jan, A.; Adolfsson, O.; Allaman, I.; Buccarello, A. L.; Magistretti, P. J.; Pfeifer, A.; Muhs, A.; Lashuel, H. A. Aβ42 Neurotoxicity Is Mediated by Ongoing Nucleated Polymerization Process Rather than by Discrete Aβ42 Species. *J. Biol. Chem.* **2011**, *286* (10), 8585−8596.
(51) Bode, D. C.; Freeley, M.; Nield, J.; Palma, M.; Viles, J. H. Amyloid-β Oligomers Have a Profound Detergent-like Effect on Lipid Membrane Bilayers, Imaged by Atomic Force and Electron Microscopy. *J. Biol. Chem.* **2019**, *294* (19), 7566−7572.
(52) Tian, Y.; Liang, R.; Kumar, A.; Szwedziak, P.; Viles, J. H. 3D-Visualization of Amyloid-β Oligomer Interactions with Lipid Membranes by Cryo-Electron Tomography. *Chem. Sci.* **2021**, *12* (20), 6896−6907.
(53) Pike, C. J.; Walencewicz-Wasserman, A. J.; Kosmoski, J.; Cribbs, D. H.; Glabe, C. G.; Cotman, C. W. Structure-Activity Analyses of β-Amyloid Peptides: Contributions of the B25-35 Region to Aggregation and Neurotoxicity. *J. Neurochem.* **1995**, *64* (1), 253−265.
(54) Mirzabekov, T.; Lin, M. C.; Yuan, W. L.; Marshall, P. J.; Carman, M.; Tomaselli, K.; Lieberburg, I.; Kagan, B. L. Channel Formation in Planar Lipid Bilayers by a Neurotoxic Fragment of the β-Amyloid Peptide. *Biochem. Biophys. Res. Commun.* **1994**, *202* (2), 1142−1148.
(55) Kandel, N.; Zheng, T.; Huo, Q.; Tatulian, S. A. Membrane Binding and Pore Formation by a Cytotoxic Fragment of Amyloid β Peptide. *J. Phys. Chem. B* **2017**, *121* (45), 10293−10305.
(56) Bhowmik, D.; Mote, K. R.; MacLaughlin, C. M.; Biswas, N.; Chandra, B.; Basu, J. K.; Walker, G. C.; Madhu, P. K.; Maiti, S. Cell-

Membrane-Mimicking Lipid-Coated Nanoparticles Confer Raman Enhancement to Membrane Proteins and Reveal Membrane-Attached Amyloid-β Conformation. *ACS Nano* **2015**, *9* (9), 9070−9077.
(57) Serra-Batiste, M.; Ninot-Pedrosa, M.; Bayoumi, M.; Gairí, M.; Maglia, G.; Carulla, N. Aβ42 Assembles into Specific β-Barrel Pore-Forming Oligomers in Membrane-Mimicking Environments. *Proc. Natl. Acad. Sci. U. S. A.* **2016**, *113* (39), 10866−10871.
(58) Österlund, N.; Moons, R.; Ilag, L. L.; Sobott, F.; Graslund, A. Native Ion Mobility-Mass Spectrometry Reveals the Formation of B-barrel Shaped Amyloid-β Hexamers in a Membrane-Mimicking Environment. *J. Am. Chem. Soc.* **2019**, *141* (26), 10440−10450.
(59) Ciudad, S.; Puig, E.; Botzanowski, T.; Meigooni, M.; Arango, A. S.; Do, J.; Mayzel, M.; Bayoumi, M.; Chaignepain, S.; Maglia, G.; et al. Aβ(1-42) Tetramer and Octamer Structures Reveal Edge Conductivity Pores as a Mechanism for Membrane Damage. *Nat. Commun.* **2020**, *11* (1), 3014.
(60) Wu, J.; Blum, T. B.; Farrell, D. P.; DiMaio, F.; Abrahams, J. P.; Luo, J. Cryo-Electron Microscopy Imaging of Alzheimer's Amyloid-Beta 42 Oligomer Displayed on a Functionally and Structurally Relevant Scaffold. *Angew. Chem., Int. Ed.* **2021**, *60* (34), 18680−18687.
(61) Durell, S. R.; Guy, H. R.; Arispe, N.; Rojas, E.; Pollard, H. B. Theoretical Models of the Ion Channel Structure of Amyloid Beta-Protein. *Biophys. J.* **1994**, *67* (6), 2137−2145.
(62) Shafrir, Y.; Durell, S.; Arispe, N.; Guy, H. R. Models of Membrane-Bound Alzheimer's Abeta Peptide Assemblies. *Proteins: Struct., Funct., Bioinf.* **2010**, *78* (16), 3473−3487.
(63) Durell, S. R.; Kayed, R.; Guy, H. R. The Amyloid Concentric β-Barrel Hypothesis: Models of Amyloid Beta 42 Oligomers and Annular Protofibrils. *Proteins: Struct., Funct., Bioinf.* **2022**, *90* (5), 1190−1209.
(64) Jang, H.; Zheng, J.; Nussinov, R. Models of Beta-Amyloid Ion Channels in the Membrane Suggest That Channel Formation in the Bilayer Is a Dynamic Process. *Biophys. J.* **2007**, *93* (6), 1938−1949.
(65) Jang, H.; Arce, F. T.; Capone, R.; Ramachandran, S.; Lal, R.; Nussinov, R. Misfolded Amyloid Ion Channels Present Mobile Beta-Sheet Subunits in Contrast to Conventional Ion Channels. *Biophys. J.* **2009**, *97* (11), 3029−3037.
(66) Jang, H.; Teran Arce, F.; Ramachandran, S.; Kagan, B. L.; Lal, R.; Nussinov, R. Familial Alzheimer's Disease Osaka Mutant (ΔE22) β-Barrels Suggest an Explanation for the Different Aβ1-40/42 Preferred Conformational States Observed by Experiment. *J. Phys. Chem. B* **2013**, *117* (39), 11518−11529.
(67) Jang, H.; Connelly, L.; Teran Arce, F.; Ramachandran, S.; Kagan, B. L.; Lal, R.; Nussinov, R. Mechanisms for the Insertion of Toxic, Fibril-like β-Amyloid Oligomers into the Membrane. *J. Chem. Theory Comput.* **2013**, *9* (1), 822−833.
(68) Nguyen, P. H.; Campanera, J. M.; Ngo, S. T.; Loquet, A.; Derreumaux, P. Tetrameric Aβ40 and Aβ42 β-Barrel Structures by Extensive Atomistic Simulations. I. in a Bilayer Mimicking a Neuronal Membrane. *J. Phys. Chem. B* **2019**, *123* (17), 3643−3648.
(69) Ngo, S. T.; Nguyen, P. H.; Derreumaux, P. Impact of the Rat R5G, Y10F, and H13R Mutations on Tetrameric Aβ42 β-Barrel in a Lipid Bilayer Membrane Model. *J. Phys. Chem. B* **2021**, *125* (12), 3105−3113.
(70) Sun, Y.; Kakinen, A.; Wan, X.; Moriarty, N.; Hunt, C. P. J.; Li, Y.; Andrikopoulos, N.; Nandakumar, A.; Davis, T. P.; Parish, C. L.; et al. Spontaneous Formation of β-Sheet Nano-Barrels during the Early Aggregation of Alzheimer's Amyloid Beta. *Nano Today* **2021**, *38*, 101125.
(71) Sepehri, A.; Nepal, B.; Lazaridis, T. Distinct Modes of Action of IAPP Oligomers on Membranes. *J. Chem. Inf. Model.* **2021**, *61* (9), 4645−4655.
(72) Lazaridis, T. Effective Energy Function for Proteins in Lipid Membranes. *Proteins: Struct., Funct., Bioinf.* **2003**, *52* (2), 176−192.
(73) Lazaridis, T.; Karplus, M. Effective Energy Function for Proteins in Solution. *Proteins: Struct., Funct., Bioinf.* **1999**, *35* (2), 133−152.
(74) Mihajlovic, M.; Lazaridis, T. Antimicrobial Peptides Bind More Strongly to Membrane Pores. *Biochim. Biophys. Acta, Biomembr.* **2010**, *1798* (8), 1494−1502.
(75) Lazaridis, T. Structural Determinants of Transmembrane Beta-Barrels. *J. Chem. Theory Comput.* **2005**, *1* (4), 716−722.
(76) Martyna, G. J.; Tobias, D. J.; Klein, M. L. Constant Pressure MD Algorithms. *J. Chem. Phys.* **1994**, *101* (5), 4177−4189.
(77) Yanagisawa, K. Pathological Significance of Ganglioside Clusters in Alzheimer's Disease. *J. Neurochem.* **2011**, *116* (5), 806−812.
(78) Matsuzaki, K. Aβ − Ganglioside Interactions in the Pathogenesis of Alzheimer ' s Disease. *Biochim. Biophys. Acta, Biomembr.* **2020**, *1862* (8), 183233.
(79) Petkova, A. T.; Yau, W. M.; Tycko, R. Experimental Constraints on Quaternary Structure in Alzheimer's β-Amyloid Fibrils. *Biochemistry* **2006**, *45* (2), 498−512.
(80) Jang, H.; Arce, F. T.; Ramachandran, S.; Capone, R.; Lal, R.; Nussinov, R. Beta-Barrel Topology of Alzheimer's Beta-Amyloid Ion Channels. *J. Mol. Biol.* **2010**, *404* (5), 917−934.
(81) Hoyer, W.; Grönwall, C.; Jonsson, A.; Ståhl, S.; Härd, T. Stabilization of a β-Hairpin in Monomeric Alzheimer's Amyloid-β Peptide Inhibits Amyloid Formation. *Proc. Natl. Acad. Sci. U. S. A.* **2008**, *105* (13), 5099−5104.
(82) Kakeshpour, T.; Ramanujam, V.; Barnes, C. A.; Shen, Y.; Ying, J.; Bax, A. A Lowly Populated, Transient β-Sheet Structure in Monomeric Aβ1-42 Identified by Multinuclear NMR of Chemical Denaturation. *Biophys. Chem.* **2021**, *270* (March), 106531.
(83) Lipkin, R.; Pino-Angeles, A.; Lazaridis, T. Transmembrane Pore Structures of β-Hairpin Antimicrobial Peptides by All-Atom Simulations. *J. Phys. Chem. B* **2017**, *121* (39), 9126−9140.
(84) Sticht, H.; Bayer, P.; Willbold, D.; Dames, S.; Hilbich, C.; Beyreuther, K.; Frank, R. W.; Rosch, P. Structure of Amyloid A4 (1-40)-Peptide of Alzheimer's Disease. *Eur. J. Biochem.* **1995**, *233*, 293−298.
(85) Hassan, R.; Abedin, F.; Tatulian, S. A. Structure of Unmodified and Pyroglutamylated Amyloid Beta Peptides in Lipid Membranes. *Biophys. J.* **2022**, *121*, 328a.
(86) Marchesi, V. T. An Alternative Interpretation of the Amyloid Aβ_hypothesis with Regard to the Pathogenesis of Alzheimer's Disease. *Proc. Natl. Acad. Sci. U. S. A.* **2005**, *102* (26), 9093−9098.
(87) Sepehri, A.; PeBenito, L.; Pino-Angeles, A.; Lazaridis, T. What Makes a Good Pore Former: A Study of Synthetic Melittin Derivatives. *Biophys. J.* **2020**, *118* (8), 1901−1913.
(88) Arispe, N.; Pollard, H. B.; Rojas, E. Giant Multilevel Cation Channels Formed by Alzheimer Disease Amyloid β- Protein [AβP-(1-40)] in Bilayer Membranes. *Proc. Natl. Acad. Sci. U. S. A.* **1993**, *90* (22), 10573−10577.
(89) Hirakura, Y.; Lin, M. C.; Kagan, B. L. Alzheimer Amyloid Aβ1-42 Channels: Effects of Solvent, PH, and Congo Red. *J. Neurosci. Res.* **1999**, *57* (4), 458−466.
(90) Quist, A.; Doudevski, I.; Lin, H.; Azimova, R.; Ng, D.; Frangione, B.; Kagan, B.; Ghiso, J.; Lal, R. Amyloid Ion Channels: A Common Structural Link for Protein-Misfolding Disease. *Proc. Natl. Acad. Sci. U. S. A.* **2005**, *102* (30), 10427−10432.
(91) Rhee, S. K.; Quist, A.; Lal, R. Amyloid β Protein-(1− 42) Forms Calcium-Permeable, Zn2+-Sensitive Channel. *J. Biol. Chem.* **1998**, *273* (22), 13379−13383.
(92) Arispe, N.; Pollard, H. B.; Rojas, E. Zn2+ Interaction with Alzheimer Amyloid β Protein Calcium Channels. *Proc. Natl. Acad. Sci. U. S. A.* **1996**, *93* (4), 1710−1715.
(93) Kawahara, M.; Arispe, N.; Kuroda, Y.; Rojas, E. Alzheimer's Disease Amyloid β-Protein Forms Zn2+-Sensitive, Cation- Selective Channels across Excised Membrane Patches from Hypothalamic Neurons. *Biophys. J.* **1997**, *73* (1), 67−75.
(94) Díaz, J. C.; Linnehan, J.; Pollard, H.; Arispe, N. Histidines 13 and 14 in the Aβ Sequence Are Targets for Inhibition of Alzheimer's Disease Aβ Ion Channel and Cytotoxicity. *Biol. Res.* **2006**, *39* (3), 447−460.

https://doi.org/10.1021/acschemneuro.2c00535
ACS Chem. Neurosci. 2023, 14, 99−110

(95) Demuro, A.; Mina, E.; Kayed, R.; Milton, S. C.; Parker, I.; Glabe, C. G. Calcium Dysregulation and Membrane Disruption as a Ubiquitous Neurotoxic Mechanism of Soluble Amyloid Oligomers. *J. Biol. Chem.* **2005**, *280* (17), 17294−17300.
(96) Bode, D. C.; Baker, M. D.; Viles, J. H. Ion Channel Formation by Amyloid-B42 Oligomers but Not Amyloid-B40 in Cellular Membranes. *J. Biol. Chem.* **2017**, *292* (4), 1404−1413.
(97) Bi, C.; Bi, S.; Li, B. Processing of Mutant β-Amyloid Precursor Protein and the Clinicopathological Features of Familial Alzheimer's Disease. *Aging Dis.* **2019**, *10* (2), 383−403.
(98) Ngo, S. T.; Derreumaux, P.; Vu, V. V. Probable Transmembrane Amyloid α-Helix Bundles Capable of Conducting Ca 2+ Ions. *J. Phys. Chem. B* **2019**, *123* (12), 2645−2653.
(99) Cline, E. N.; Bicca, M. A.; Viola, K. L.; Klein, W. L. The Amyloid-β Oligomer Hypothesis: Beginning of the Third Decade. *J. Alzheimer's Dis.* **2018**, *64* (s1), S567−S610.
(100) Sandberg, A.; Luheshi, L. M.; Söllvander, S.; De Barros, T. P.; Macao, B.; Knowles, T. P. J.; Biverstål, H.; Lendel, C.; Ekholm-Petterson, F.; Dubnovitsky, A.; et al. Stabilization of Neurotoxic Alzheimer Amyloid-β Oligomers by Protein Engineering. *Proc. Natl. Acad. Sci. U. S. A.* **2010**, *107* (35), 15595−15600.
(101) Lendel, C.; Bjerring, M.; Dubnovitsky, A.; Kelly, R. T.; Filippov, A.; Antzutkin, O. N.; Nielsen, N. C.; Härd, T. A Hexameric Peptide Barrel as Building Block of Amyloid-β Protofibrils. *Angew. Chem., Int. Ed.* **2014**, *53* (47), 12756−12760.
(102) Kayed, R.; Head, E.; Thompson, J. L.; McIntire, T. M.; Milton, S. C.; Cotman, C. W.; Glabe, C. G. Common Structure of Soluble Amyloid Oligomers Implies Common Mechanism of Pathogenesis. *Science* **2003**, *300* (5618), 486−489.
(103) Yoshiike, Y.; Kayed, R.; Milton, S. C.; Takashima, A.; Glabe, C. G. Pore-Forming Proteins Share Structural and Functional Homology with Amyloid Oligomers. *NeuroMol. Med.* **2007**, *9* (3), 270−275.

NOTE ADDED AFTER ASAP PUBLICATION

This paper was published ASAP on December 16, 2022, with errors in Figure 5. The corrected version was reposted on December 20, 2022.

https://doi.org/10.1021/acschemneuro.2c00535
ACS Chem. Neurosci. 2023, 14, 99−110